Real-Time Observations of Microtubule Dynamic Instability in Living Cells

L. Cassimeris, Nancy K. Pryer, and E. D. Salmon

Department of Biology, University of North Carolina, Chapel Hill, North Carolina 27599-3280

Abstract. Individual microtubule dynamics were observed in real time in primary cultures of newt lung epithelium using video-enhanced differential interference contrast microscopy and digital image processing. The linear filaments observed in cells corresponded to microtubules based on three criteria: (*a*) small particles translocated along them; (*b*) the majority of them disappeared after incubation in nocodazole; (*c*) and the distribution observed by differential interference contrast correlated with anti-tubulin immunofluorescence staining of the same cell. Microtubules were most clearly observed at the leading edge of cells located at the periphery of the epithelial sheet. Microtubules exhibited dynamic instability behavior: individual microtubules existed in persistent phases of elongation or rapid shortening. Microtubules elongated at a velocity of 7.2 μm/min ± 0.3 SEM (n = 42) and rapidly shortened at a velocity of 17.3 μm/min ± 0.7 SEM (n = 35). The transitions between elongation and rapid shortening occurred abruptly and stochastically with a transition frequency of 0.014 s^{-1} for catastrophe and 0.044 s^{-1} for rescue. Approximately 70% of the rapidly shortening microtubules were rescued and resumed elongation within the 35 × 35 μm microscopic field. A portion of the microtubule population appeared differentially stable and did not display any measurable elongation or shortening during 10–15-min observations.

THE great majority of cellular microtubules are labile polymers that exist in an equilibrium with a cytoplasmic pool of tubulin subunits (11, 23, 27). Dynamic microtubule polymers are essential for the rapid rearrangements of the microtubule cytoskeleton which occur during the transitions between the interphase and mitosis portions of the cell cycle. In addition, dynamic remodeling of microtubules is important in cell morphogenesis and directed cell motility (5, 6, 33).

Although several models have been proposed to explain the mechanism of microtubule assembly behavior, studies of highly purified tubulin have identified dynamic instability as the mechanism of microtubule assembly dynamics in vitro (4, 9, 13, 15, 16, 24, 36). In this model microtubules exist in one of two phases: they are either elongating or rapidly shortening, with rare, abrupt, and random transitions between these phases. The entire microtubule population behaves heterogeneously because these transitions occur randomly; at any given time most microtubules will be growing at a relatively slow rate while fewer microtubules will be shortening at a relatively faster rate (15, 16).

Recently, Horio and Hotani (9), Walker et al. (36), and Salmon et al. (24) have directly visualized the dynamic instability behavior of microtubules in vitro, in real time, using light microscopic methods. These real-time observations have provided essential information on the dynamic instability behavior of microtubules that could not be obtained from analysis of samples fixed at time points. Detailed analysis of microtubule assembly by Walker et al. (36) has led to the following model of the dynamic history of a microtubule in vitro undergoing dynamic instability: a microtubule is initiated at a nucleating center (an axoneme fragment or a centrosome) and elongates at constant velocity for a variable length of time. It then undergoes an abrupt transition (catastrophe) and rapidly shortens at constant velocity. A rapidly shortening microtubule may either completely disassemble or undergo an abrupt transition (rescue) and resume elongation. Real-time observations of microtubule assembly at video frame rates (30 frames/s) enabled Walker et al. (36) to determine accurately the rates of elongation and rapid shortening, the frequencies of catastrophe and rescue, and the kinetic constants for the association and dissociation reactions (36).

Studies of microtubule dynamics in vivo suggest that dynamic instability is also the mechanism of microtubule assembly within the cell. First, fluorescence photobleaching studies have shown that the tubulin subunits within microtubules rapidly exchange with the cytoplasmic subunit pool (23, 26, 27). Second, when microtubule assembly in cells is blocked with the drug nocodazole, the resulting rate and pattern of microtubule disassembly is rapid and occurs heterogeneously within the microtubule population (3). Third, when labeled tubulin subunits are injected into cells, assem-

L. Cassimeris' present address is Department of Biology, University of Pennsylvania, Philadelphia, PA 19104. N. Pryer's present address is Department of Biochemistry, University of California, Berkeley, CA 94720.

bly of labeled segments occurs on the distal ends of preexisting microtubules and from new microtubules elongating from the centrosome (28, 29, 31).

Recently, Sammak and Borisy (25) reported observations of microtubule dynamic instability in living cells by following the behavior of microtubules which had incorporated rhodamine-labeled tubulin. The major limitations of this study were the long time intervals (1.4 ± 0.8 min) between the recording of successive fluorescent images and the possible effects of microinjected rhodamine-tubulin analogues on the natural dynamics of cytoplasmic microtubules (34). Because of the long intervals between samples, the microtubule excursions demonstrated by this method are likely to be an underestimate of the true dynamic nature of the microtubules.

In this study we describe observations of individual microtubule assembly dynamics obtained in living cells in real time (0.033 s video frame rate) using video-enhanced differential interference contrast (DIC)[1] microscopy and digital image processing (1, 10, 12). These observations clearly demonstrate that microtubules in vivo exhibit dynamic instability behavior. In addition, we have measured the rates of elongation and rapid shortening of individual microtubules and obtained estimates of the frequency of transition between phases. These real-time observations of dynamic instability in vivo allow an accurate determination of individual microtubule behavior, which was not previously possible using measurements of the average behavior of populations of microtubules.

Materials and Methods

Newt lung culture

Primary cultures of newt lung epithelial cells were grown on glass coverslips as described by Rieder et al. (21). Cells were maintained at room temperature (23°C) and were used on the fourth or fifth day after each culture was begun.

Light microscopy

For DIC observations coverslips were mounted on glass slides with small pieces of parafilm as spacers, and sealed with valap (beeswax, lanolin, and petrolatum in a 1:1:1 mixture). Typically, small regions of the cells were observed for 10–15 min.

The microscope equipped for high resolution DIC, video, and digital enhancement has been described previously (19, 24, 37). Briefly, cells were observed with a 100×/1.25 NA Zeiss Plan lens, appropriate Zeiss DIC prisms, and 1.4 NA Zeiss condenser on a Zeiss photomicroscope I. To protect cells from deleterious illumination effects, heat-cut and 546-nm interference filters were used. No changes in cell behavior were noticed over the course of our observations. Furthermore, mitotic newt cells followed for 2–3 h under constant illumination with the same microscope system progressed normally through mitosis.

Images were projected onto a video camera (model 67; Dage-MTI Inc., Wabash, MI) and then digitally enhanced with a laboratory-built image processor that consisted of Max Video (Datacube, Peabody, MA) digital image processing boards installed in a bus computer (model VME; Force Inc., Los Gatos, CA). A real-time exponential average of two frames and background subtraction were used to reduce electronic noise (37). Images were recorded on video tape using a tape recorder (model 5800 H, 3/4″; Sony Corporation of America, Park Ridge, NJ). Micrographs were made by photographing the image from a video monitor using Pan-X film (Eastman Kodak Co., Rochester, NY).

1. *Abbreviation used in this paper*: DIC, differential interference contrast.

Nocodazole perfusion

Cells were perfused with a solution of 10 μg/ml nocodazole (Sigma Chemical Co., St. Louis, MO) in culture medium. Nocodazole was prepared as a 10-mg/ml stock solution in DMSO and stored at −20°C.

Immunofluorescence

For immunofluorescent localization of tubulin, cells previously observed using DIC were perfused with a fixative solution (0.5% glutaraldehyde in 80 mM Pipes, 5 mM EGTA, 0.5 mM $MgCl_2$, pH 6.9) and fixed for 5–10 min on the microscope stage. The area of interest was marked with a circular diamond scribe and the coverslip was removed from the slide, rinsed in PBS (8 mM Na_2HPO_4, 1.5 mM KH_2PO_4, 0.137 M NaCl, and 2.7 mM KCl, pH 7.3), and postfixed in ice-cold methanol for 5 min. After fixation each coverslip was processed for anti-tubulin immunofluorescence as described previously (3).

Data analysis

Rates of microtubule elongation and rapid shortening were measured from real-time tape recordings using an Apple II computer analysis system described previously (19, 37). Although the video recordings have a time resolution of 0.033 s, the measurement time resolution during analysis was approximately one-half second due to microtubule movements in and out of focus.

Results

We observed the dynamic instability of linear filaments in primary cultures of newt lung epithelial cells using video-enhanced DIC microscopy and digital image processing (see Figs. 1, 2, 3, and 6). These linear filaments were most clearly visualized in cells located at the edges of the epithelial sheet, distal from the tissue explant. Because cells in the central regions of the epithelial sheet tend to overlap slightly, it was not always possible to see filament ends with clarity in these cells. In addition, filaments could only be observed in ~10–20% of the cells of any given culture. Within a cell where we could clearly observe linear filaments there were also areas where we could not see these filaments. For example, it was not possible to track filaments with certainty into the dense central regions of the cell. We have limited our observations to the thin cytoplasm at the periphery of cells located at the edge of the epithelial sheet, and we have observed an area ~35 × 35 μm at the edge of the cell.

The linear filaments corresponded to microtubules by three criteria. First, we observed saltatory translocation of small particles along the filaments, and particle movement is known to occur along microtubules in animal cells (30). Fig. 1 shows the movements of an oblong particle, probably a mitochondrion, along a linear filament. As the linear filament bends (Fig. 1, *d* and *e*) the particle remains attached and takes on the contour of the filament. For any given particle, movement was bi-directional as well as saltatory (Fig. 1, *e* and *f*).

Second, treatment of newt lung epithelial cells with the drug nocodazole, which promotes microtubule disassembly, resulted in a significant reduction in the number of filaments. After ~20 min in nocodazole-containing medium, 70–90% of the linear filaments were no longer present (data not shown). Due to focus changes during perfusion, it was not possible to record nocodazole-induced microtubule disassembly in real time.

Third, the linear filaments observed using DIC microscopy correlate with anti-tubulin immunofluorescent staining of the same cell. Fig. 2 shows a portion of a cell observed

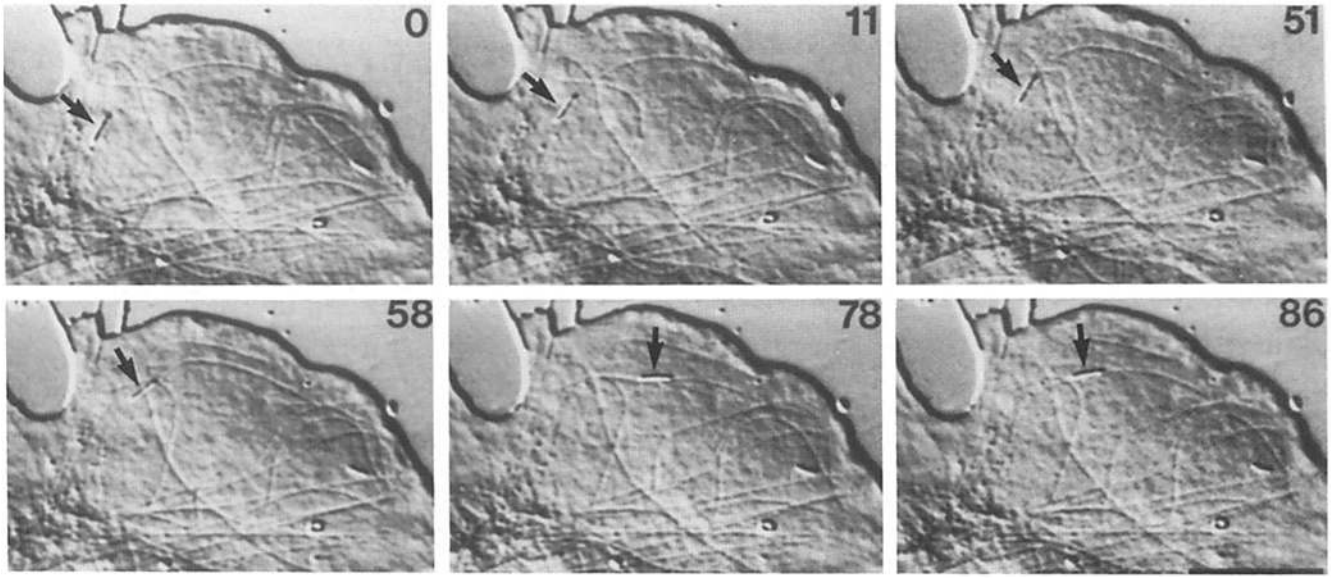

Figure 1. A series of digital and video-enhanced DIC micrographs taken from a real-time video tape recording showing the translocation of a particle (*arrow*) along a linear filament. The time in seconds is given in each frame. Bar, 10 μm.

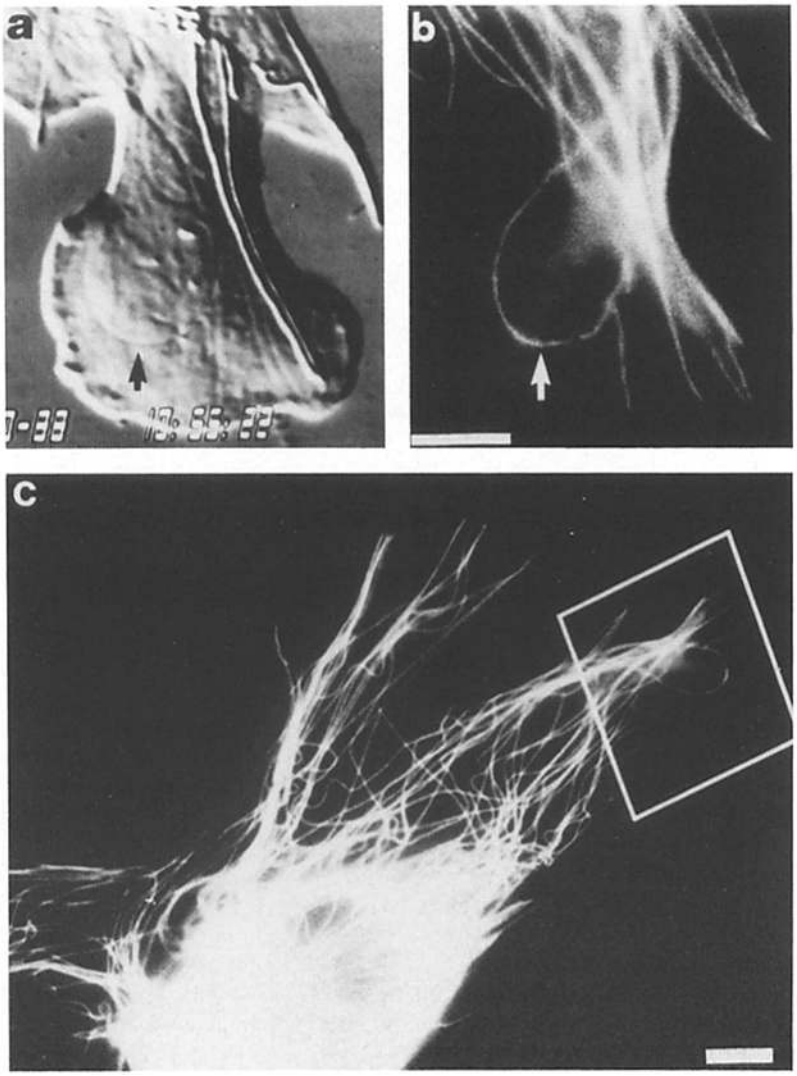

Figure 2. (*a*) Micrograph of a region of a cell viewed with video-enhanced DIC microscopy and digital image processing ~1 min before fixation. Many linear filaments are present. (*b*) The corresponding immunofluorescent micrograph of the same area of the cell after fixation and staining for tubulin. The microtubules present in this micrograph correlate with the linear filaments in *a*. One filament in the DIC micrograph disassembled before fixation (*arrowhead*, *a*). Note the distinctive curved filament in *a* and the corresponding microtubule in *b* (*arrows*). (*c*) Immunofluorescent micrograph of the cell shown in *b*. This micrograph shows the overall distribution of microtubules in the cell. The area within the white box corresponds to the area observed by DIC microscopy. Bars: (*a* and *b*) 5 μm; (*c*) 10 μm.

with DIC microscopy ~1 min before fixation (Fig. 2 *a*) and the corresponding microtubule image (Fig. 2 *b*). The linear elements present in the DIC image correlate with microtubules in the immunofluorescent image. A distinct bent microtubule (*arrow*) is clearly present in both images. Fewer microtubules are seen in the DIC image than in the immunofluorescent image because of the extremely shallow depth of field of DIC microscopy.

Hayden and Allen (7) used correlative DIC light microscopy and whole mount electron microscopy to demonstrate that individual microtubules can be observed in living cells using video-enhanced DIC microscopy. In addition, Osborn and Weber (18) have shown that the immunofluorescent images of microtubules at the periphery of cells are equivalent to individual microtubules. If a tight cluster of multiple microtubules were responsible for generating the linear filaments in our DIC images then the immunofluorescent images would be brighter than the corresponding images of single microtubules (Fig. 2). We found that for any individual linear filament observed with DIC, the corresponding immunofluorescent image had the intensity of a single microtubule, indicating that the linear filaments observed by DIC corresponded to individual microtubules.

Based on the behavior of the linear filaments observed by DIC microscopy, microtubule assembly behavior in these cells is best described by the dynamic instability model. Many individual microtubules were observed to elongate or rapidly shorten, as shown in Fig. 3. Several dynamic microtubules are shown in this series of micrographs taken from a real-time recording. One microtubule (*solid arrowhead*) elongated (Fig. 3 *a*) until it reached the cell margin (*b*), rapidly shortened (*c*), and then elongated again (*d–f*). Another microtubule (*open arrow*) also elongated (Fig. 3, *a–c*) until it reached the cell margin and then rapidly shortened (*d–f*). Several other microtubules in the field also exhibited dynamic instability. A differentially stable microtubule was also present (*white arrowhead*, Fig. 3, *b–f*).

Many microtubules exhibited repeated cycles of elongation and rapid shortening during the time of observation. Some microtubules elongated to the cell margin before rapidly shortening, but in many cases rapid shortening began before elongation proceeded to the cell margin (Fig. 4, *a*, *b*, and *c*). In addition, many microtubules that elongated to the cell margin appeared to bend away from the edge of the cell and continued elongating. Occasionally, microtubules were observed to elongate into the field of view from more central regions of the cell (data not shown).

To determine elongation and rapid shortening rates, the ends of individual dynamic microtubules were tracked in real time using a computer-driven analysis system. We were careful to analyze only those microtubules where we could unambiguously track the microtubule end during elongation or rapid shortening. This analysis excluded microtubules whose length changes were below our limit of resolution (0.5 μm) and these were regarded as stable. Fig. 4 shows four dynamic history graphs for microtubules analyzed by this method. Although the video recordings have a time resolution of 0.033 s, the actual time resolution during analysis was ~0.5 s because the microtubule ends moved in and out of focus. Microtubule ends could be followed for distances up to 25 μm. Fig. 4 *a* shows the behavior of one microtubule shown in Fig. 3 (*solid arrowhead*) over a longer time inter-

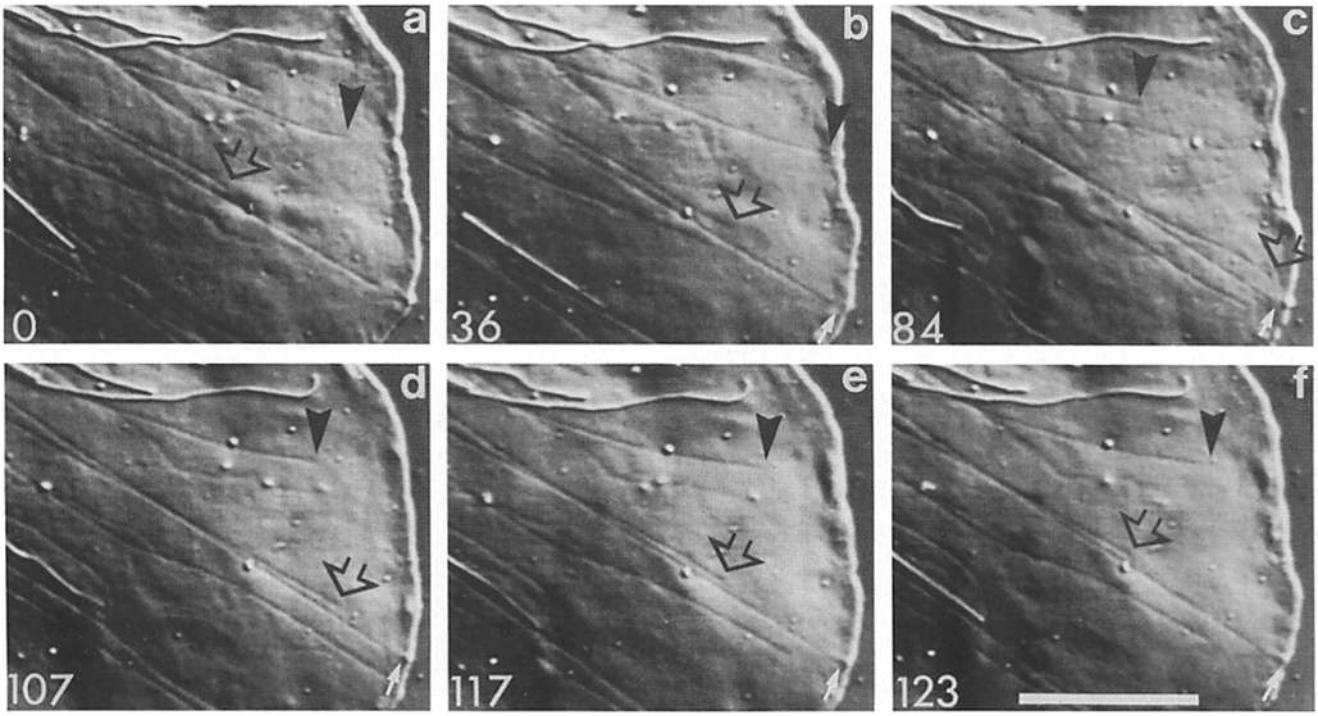

Figure 3. A series of micrographs taken from a real-time video tape recording to demonstrate the dynamic assembly and disassembly of microtubules. A microtubule (*black arrowhead*) elongates to the cell margin (*a* and *b*), rapidly shortens (*b* and *c*), is rescued, and resumes elongation (*d–f*). Another microtubule (*open arrow*) elongates (*a–c*) to the cell margin and rapidly shortens (*d–f*). A differentially stable microtubule (*white arrow*) is also present (*b–f*). The time in seconds is given in each frame. Bar, 10 μm.

Table I. Dynamic Instability of Newt Lung Cell Microtubules

	Elongation	Rapid shortening	Catastrophe	Rescue
Rate (μm/min)*	7.2 ± 0.3 (42)	17.3 ± 0.7 (35)	n.a.	n.a.
L (μm)‡	8.5 ± 7.0 (14)	6.5 ± 4.3 (19)	n.a.	n.a.
t (s)‡	71 ± 61 (14)	22 ± 15 (19)	n.a.	n.a.
k (s^{-1})§	n.a.	n.a.	0.014	0.044

* Mean rate ± SEM (SEM is determined from SD/$\sqrt{n}$) determined from the slopes of dynamic history graphs. Numbers in parentheses are the number of observed events.
‡ Length of the mean microtubule length excursion (L) and time spent in each phase (t) ± SD determined as described in the text. Numbers in parentheses are the number of observed events.
§ Transition frequencies between phases, determined as described in the text.
n.a., not applicable.

val. As shown by these dynamic history graphs, individual microtubules underwent repeated phases of elongation and rapid shortening, with each phase occurring at a relatively constant velocity.

The mean rate of microtubule elongation, determined from the slopes of dynamic history curves (Fig. 4) of 42 elongation events in 17 cells, was 7.2 μm/min ± 0.3 SEM (Table I). The histogram of the distribution of elongation rates (Fig. 5) shows little variation.

Rapid shortening proceeded at a mean rate of 17.3 μm/min ± 0.7 SEM (based on 35 events in 15 cells), a rate 2.5 times faster than the rate of elongation (Table I). The histogram of rapid shortening rates shows a greater variation in rates than that found for assembly (Fig. 5). There appears to be a broad, continuous range of shortening rates. We cannot explain this broad distribution, but the variation could be due to a differential cellular distribution of unknown microtubule stabilizing factors.

Transitions between phases were abrupt and asynchronous for the observable microtubules of a given cell (Figs. 3 and 4). To determine the frequency of catastrophe we measured the time individual microtubules spent in the elongation phase before a transition (catastrophe) to the rapid shortening phase. A mean time was calculated from 14 samples where we could clearly observe the entire elongation phase (for example, from 85 to 160 s in Fig. 4 *a*). The mean time of elongation before catastrophe was 71 ± 61 s (Table I). The high standard deviation indicates that catastrophe is a stochastic process. The frequency of catastrophe (0.014 s^{-1}; Table I) was determined from the inverse of the mean time spent in the elongation phase.

The frequency of rescue (the transition from rapid shortening to elongation) was determined by the same method. The mean time a microtubule spent in the rapid shortening phase was 21 ± 15 s Table I). The high standard deviation again indicates that rescue is also a stochastic process. The frequency of rescue (0.044 s^{-1}; Table I) was much higher than the frequency of catastrophe. The majority of microtubules in the rapid shortening phase were rescued within the field of view. We estimate that 70% of the rapidly shortening

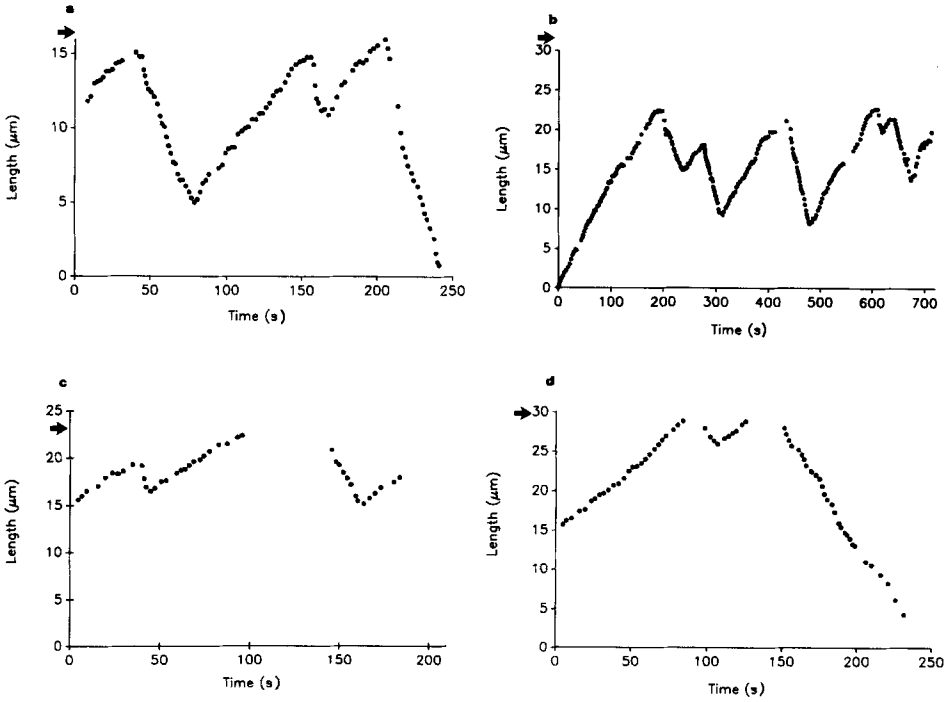

Figure 4. Four dynamic history graphs of individual microtubule assembly dynamics. In each graph the position of the microtubule end is plotted vs. time (in seconds). Since 90% of the cells showed little or no movement, a point along the edge of the video screen was used as a reference point and each data point is a measure of the distance of the microtubule end from the edge of the video screen at a particular time point. The time resolution during analysis is ~0.5 s due to variations in focus. The longer intervals between points represent periods of time when the microtubule end was obscured by the cell margin or other microtubules, or when the microtubule end was out of focus. On each graph the approximate position of the cell margin is noted with an arrow on the *y*-axis. Microtubules exist in persistent phases of either elongation or rapid shortening with each phase proceeding at relatively constant velocity. The transitions between phases are abrupt.

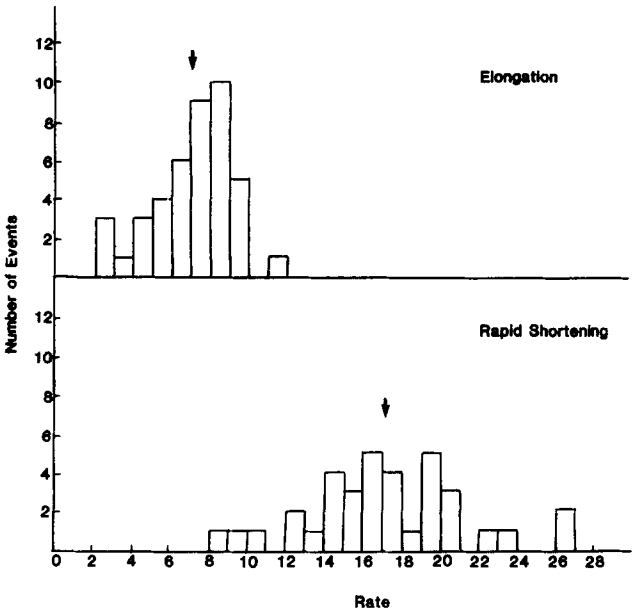

Figure 5. Histograms of microtubule elongation and rapid shortening rates determined from dynamic history graphs (see Fig. 4). Arrows denote the mean rate of either elongation or rapid shortening.

microtubules were rescued within ~35 μm of the cell periphery.

A portion of the microtubule population appeared differentially stable (Fig. 3), confirming previous reports of a subpopulation of stable microtubules (3, 26, 27, 28, 29) in interphase cells. If stable microtubules elongate and/or shorten the length of these excursions is below our limit of resolution (0.5 μm). It has not been possible to determine the exact percentages of labile and differentially stable microtubules because not all microtubule ends are clearly visible in a single microscopic field.

In addition to the assembly behavior described above, we have observed lateral and bending movements of microtubules. Although microtubules move laterally they rarely appeared to form contacts with neighboring microtubules. Microtubules occasionally formed bends (Fig. 6), but whether this bending is the result of continued microtubule assembly once the microtubule reached an obstruction (such as the cell margin) has not been determined. A few microtubules were observed to bend while rapidly shortening and several previously bent microtubules shortened and maintained this bent path (data not shown). The latter two observations suggest that bending can occur without concurrent microtubule growth.

Over the time course of our observations ~90% of the cells showed no appreciable movement (<5 μm). In a few cases cells appeared to extend the lamellipodium under observation, but in other cases the lamellipodium retracted. We have not observed any obvious differences in microtubule behavior correlated with these different cell behaviors.

Discussion

Newt lung epithelial cells have proven to be a useful cell type for the quantitative analysis of microtubule behavior in vivo because the length changes of individual microtubules can be accurately followed in real time using video-enhanced DIC microscopy and digital image processing. Our observations demonstrate that microtubules exist in persistent phases of either elongation or rapid shortening, with random and abrupt transitions between these phases, as described by the dynamic instability model of microtubule assembly (15, 16).

We have interpreted the observed dynamic length changes of these microtubules as representing microtubule assembly and disassembly. Because we cannot either mark a region of a microtubule or see both ends of a microtubule, we cannot directly rule out sliding of microtubules as a mechanism responsible for the observed changes in microtubule lengths. However, recent reports from several laboratories have provided strong indirect evidence that in typical animal cells microtubules are undergoing dynamic instability (3, 26, 28, 29, 31). In addition, Sammak and Borisy (25) used fluorescence photobleaching techniques to demonstrate directly that fluorescently labeled microtubules at the cell periphery do not slide. There is no evidence to suggest that centrosomal microtubules slide against each other or against a cellular matrix. Microtubule–microtubule sliding between noncentrosomal microtubules has been observed in specialized protozoa (*Reticulomyxa* and *Allogromia*) which rapidly remodel their cellular extensions (14, 32, 33). However, the rate of sliding in these cells is an order of magnitude faster than the rates of microtubule elongation and shortening observed in the present study (14, 32). Since there is overwhelming evidence that centrosomal microtubules do not slide, we have interpreted our data on microtubule length changes based solely on microtubule assembly and disassembly reactions.

Using real-time analysis, we determined that in newt lung

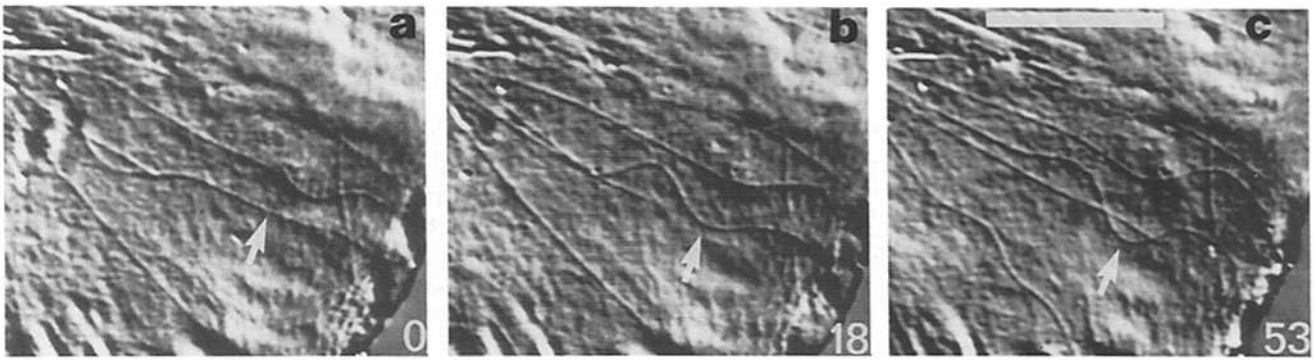

Figure 6. A series of micrographs taken from a real-time video tape recording to show bending of microtubules. One microtubule (*arrow*) clearly bends. The time in seconds is given in each frame. Bar, 10 μm.

cells at room temperature, microtubules elongate at a rate of 7.2 μm/min (189 dimers/s) and rapidly shorten at a rate of 17.3 μm/min (460 dimers/s). The dynamic history graphs (Fig. 4) show that microtubule elongation and rapid shortening proceed at relatively constant velocities. The actual data points align into nearly straight lines with very little scatter. The small amount of scatter in the data may be caused by the movement of the microtubule end laterally in the plane of focus, or in and out of the plane of focus, or from small bends in the microtubule. For example, a momentary bend would result in an apparent slower elongation rate. Conversely, relaxation of a bend would result in an apparent increase in the elongation rate. The scatter might also represent actual stochastic variations in microtubule association and dissociation reactions. Currently, we cannot differentiate between these possibilities.

Previous estimates of microtubule elongation and rapid shortening rates have been calculated from methods that sample cell populations at time points (3, 28, 29), image fluorescently labeled microtubules at time intervals (25), or lacked the resolution to identify individual microtubules (22). The results of these studies are summarized in Table II. The estimate of microtubule rapid shortening determined from real-time analysis of the reduction in birefringence of sea urchin mitotic spindles after microinjection of colchicine (22) correlates closely with the rapid shortening rate determined in this study. In contrast, elongation (28, 29) and rapid shortening (3) rates obtained by sampling cell populations at time points and data derived from fluorescent images collected at long time intervals (25) are all considerably slower than the rates determined here.

The difference in interphase microtubule assembly rates determined previously and those presented here may be explained in three ways. First, microtubule elongation and rapid shortening rates in amphibian and mammalian cells may be inherently different. Second, tubulin subunits labeled with biotin or rhodamine may alter the normal dynamics of microtubules and this effect may be critical during the illumination of fluorescently labeled microtubules (34). Third, the difference in rates may be due to the limitations of techniques with insufficient sampling frequency. Because the transitions between elongation and rapid shortening are abrupt (Fig. 4), this third possibility may contribute significantly to the differences in elongation and rapid shortening rates between this study and previous reports. A microtubule could undergo several long elongation and rapid shortening excursions, but two samples at long intervals could miss these events completely. For example, our data shows that on average, a microtubule elongates for 71 s (8.5 μm), undergoes a catastrophe, shortens for 22 s (6.5 μm), undergoes a rescue, and elongates again. If microtubules in amphibians and mammalian cells persist in elongation and rapid shortening phases for similar lengths of time, then our data suggests that within 1.5 min a microtubule could elongate 8.5 μm and shorten 6.5 μm. Observations at two time points 1.5 min apart would erroneously indicate that the microtubule's length had only changed by 2 μm.

Table II. Comparison of Microtubule Elongation and Rapid Shortening Rates In Vivo Determined by Various Methods

Cell type	Elongation	Rapid shortening	Reference
	μm/min	*μm/min*	
BSC1*	3.5	ND	28, 29
Human fibroblasts‡	3.5 ± 3.2	4.3 ± 5.7	26
Human monocytes§	ND	12	3
Sea urchin embryos‖	ND	18	22
Newt lung cells	7.2 ± 0.3	17.3 ± 0.7	This paper

* Mean rate determined from lengths of biotin-labeled microtubules in cells fixed at time points.
‡ Mean ± SD determined from fluorescent images of rhodamine-labeled microtubules collected at ~1.4-min intervals.
§ Determined from numbers of microtubules remaining in cells fixed at time points after incubation in nocodazole.
‖ Determined from real-time analysis of loss of spindle birefregence after injection of colchicine.

Using real-time observations of microtubule assembly from highly purified tubulin (16 μM) in vitro at 23°C, Walker, R. A., S. Inoue, and E. D. Salmon (unpublished observations) determined an elongation rate of 1.37 μm/min and a rapid shortening rate of 22 μm/min for microtubule plus ends. A tubulin concentration of 16 μM was selected because this is within the range of estimates of the tubulin concentration in tissue cells (8). Rapid shortening rates in vivo and in vitro are not statistically different (independent *t*-test), but the rate of elongation in vitro was ~5 times slower than the rate in vivo. Thus, the conditions in the cell must promote microtubule assembly without affecting the rate of rapid shortening. Extrapolation from studies of the effects of heat-stable porcine brain microtubule-associated proteins on microtubule assembly in vitro (Pryer, N. K., R. A. Walker, M. F. Soboeiro, and E. D. Salmon, manuscript in preparation) have shown that microtubule-associated proteins could promote the assembly of 20 μM tubulin at an elongation rate of ~7 μm/min. This corresponds well to the in vivo rate presented here. However, given these tubulin and microtubule-associated protein concentrations, and these buffer conditions in vitro, catastrophes would be extremely rare (catastrophe frequency <0.0001), and rapid shortening would proceed at half the in vivo rate. These results suggest the existence of different microtubule-associated proteins or other factors in the cell that contribute to the regulation of microtubule assembly. Factors that can promote microtubule elongation, permit a higher frequency of catastrophe, and yet not decrease the rate of microtubule rapid shortening may be important regulators of microtubule assembly.

We find that the transitions between elongation and rapid shortening are abrupt and stochastic for the dynamic population of microtubules (Fig. 4). Catastrophes occurred with a frequency of 0.014 s^{-1}, which corresponds to about one catastrophe every 71 s. The frequency of rescue was high, 0.044 s^{-1} or about one rescue every 22 s. The high frequency of rescue resulted in few rapid shortening events proceeding out of the microscopic field of view. We estimate that 70% of rapidly shortening microtubules were rescued within 35 μm of the cell edge. Sammak and Borisy (25) also found a very high frequency of rescue; ~80% of the shortening microtubules began to elongate again. Previously, we analyzed the lengths of interphase microtubules in human monocytes (3), and the histogram of microtubule lengths can be generated by dynamic instability only if rescue occurs at a high frequency. It appears that a high frequency of rescue is a characteristic of most interphase microtubules in a variety of cell types.

It is interesting to compare the data presented here for the dynamics of newt lung cell interphase microtubules with previous fluorescence photobleaching studies of microtubule turnover in newt lung cell mitotic spindles. The half-time of fluorescence recovery for bipolar spindles is ~75 s (35). Therefore, the life span of an average spindle microtubule is 108 s (derived from $t_{1/2}$/ln2), and if spindle microtubules elongate at 7 μm/min, they will elongate ~10 μm before they undergo a catastrophe. Previous experiments (17, 23) suggest that rescue occurs very infrequently for the nonkinetochore microtubules of the mitotic spindle. The rapid and uniform pattern of fluorescence recovery after photobleaching the entire half-spindle and the rapid incorporation of biotin-tubulin subunits along the entire length of nonkinetochore microtubules are both consistent with a very low frequency of rescue during mitosis. Therefore, the behavior of a nonkinetochore spindle microtubule can be summarized as follows: on average, a microtubule elongates for 82 s (108 s × fraction of time spent in elongation), undergoes a catastrophe and rapidly shortens all the weay back to the spindle pole. The time spent in the elongation phase (and therefore the frequency of catastrophe) of spindle and interphase microtubules are similar (82 and 71 s, respectively). If spindle and interphase microtubules elongate at the same rate and undergo catastrophes with approximately the same frequency, the transition between interphase and mitosis can be regulated by controlling the frequency of rescue. A high frequency of rescue during interphase allows interphase microtubules to achieve average lengths of ~70 μm. During mitosis the very low frequency of rescue means that microtubules only achieve lengths of ~10 μm (82 s × 7.1 μm/min) and this correlates well with the ~15–20-μm length of a typical newt half spindle.

In addition to the reported assembly and disassembly of microtubules, we have also observed lateral movements and bending of microtubules. These lateral and bending movements suggest that the cytomatrix is flexible enough to allow microtubule movements in the cellular regions we observed. The mechanism responsible for microtubule bending has not been determined. Some microtubules began bending once they encountered the cell margin (Fig. 6), suggesting that bending may be simply a consequence of obstructing an elongating microtubule. However, several microtubules were observed to bend while rapidly shortening and previously bent microtubules maintained their bends during rapid shortening, suggesting that microtubule elongation is not necessary to produce microtubule bends. This bending of microtubules occurred very infrequently and probably did not contribute significantly to the elongation and rapid shortening rates.

In summary, the real-time observations presented here demonstrate that the labile microtubules of newt lung epithelial cells exist in elongation or rapid shortening phases as described by the dynamic instability model of microtubule assembly. However, rescue frequency is so high that rapid shortening rarely progresses to completion, a behavior termed tempered instability by Sammak and Borisy (25, 26). Thus, most microtubule dynamics appear to occur in the peripheral 20–30 μm of the microtubule at the edge of the cell.

We are indebted to Rich Walker for many helpful discussions and for developing the microscope and image processing systems. Thanks also to Vicki Petrie and Brenda Bourns for technical assistance, and Susan Whitfield for photographic assistance. We are grateful to G. Vigers and Dick McIntosh for sharing data before publication. We would also like to thank Rich Walker, Leah Haimo, and Dick McIntosh for critically reading the manuscript. A preliminary observation of microtubules in newt lung cells was made while the authors were visiting Shinya Inoue at the Marine Biological Laboratory, Woods Hole, Masschusetts.

This work was supported by National Institutes of Health grant GM24364 to E. D. Salmon.

Received for publication 17 June 1988, and in revised form 8 August 1988.

Note Added in Proof: E. Schulze and M. Kirschner (1988. *Nature [Lond.].* 334:356–359) have achieved direct observations of microtubule dynamic instability at the periphery of living interphase BSC1 and PtK1 cells, using fluorescence methods.

References

1. Allen, R. D., N. S. Allen, and J. L. Travis. 1981. Video-enhanced contrast differential interference contrast (AVEC-DIC) microscopy: a new method capable of analyzing microtubule-related movement in the reticulopodial network of *Allogromia laticollaris*. *Cell Motil.* 1:291–302.
2. Deleted in proof.
3. Cassimeris, L. U., P. Wadsworth, and E. D. Salmon. 1986. Dynamics of microtubule depolymerization in monocytes. *J. Cell Biol.* 102:2023–2032.
4. Cassimeris, L. U., R. A. Walker, N. K. Pryer, and E. D. Salmon. 1987. Dynamic instability of microtubules. *Bioessays.* 7:149–154.
5. Daniels, M. 1975. The role of microtubules in the growth and stabilization of nerve fibers. *Annu. NY Acad. Sci.* 253:535–544.
6. Dustin, P. 1984. Microtubules. Springer-Verlag, New York. 482 pp.
7. Hayden, J. H., and R. D. Allen. 1984. Detection of single microtubules in living cells: particle transport can occur in both directions along the same microtubules. *J. Cell Biol.* 99:1785–1793.
8. Hiller, G., and K. Weber. 1978. Radioimmune assay for tubulin: a quantitative comparison of the tubulin content of different established tissue culture cells and tissues. *Cell.* 14:795–804.
9. Horio, T., and H. Hotani. 1986. Visualization of the dynamic instability of individual microtubules by dark-field microscopy. *Nature (Lond.).* 321:605–607.
10. Inoue, S. 1981. Video image processing greatly enhances contrast, quality, and speed in polarization microscopy. *J. Cell Biol.* 89:346–356.
11. Inoue, S. 1981. Cell division and the mitotic spindle. *J. Cell Biol.* 91 (Suppl.):131–147.
12. Inoue, S. 1986. Video Microscopy. Plenum Publishing Corp., New York. 584 pp.
13. Kirschner, M., and T. Mitchison. 1986. Beyond self-assembly: from microtubules to morphogenesis. *Cell.* 45:329–342.
14. Koonce, M. P., J. Tong, U. Euteneuer, and M. Schliwa. 1987. Active sliding between cytoplasmic microtubules. *Nature (Lond.).* 328:737–739.
15. Mitchison, T., and M. Kirschner. 1984. Microtubule assembly nucleated by isolated centrosomes. *Nature (Lond.).* 312:232–237.
16. Mitchison, T., and M. Kirschner. 1984. Dynamic instability of microtubule growth. *Nature (Lond.).* 312:237–242.
17. Mitchison, T., L. Evans, E. Schulze, and M. Kirschner. 1986. Sites of microtubule assembly and disassembly in the mitotic spindle. *Cell.* 45: 515–527.
18. Osborn, M., and K. Weber. 1982. Immunofluorescence and immunocytochemical procedures with affinity purified antibodies: tubulin-containing structures. *Methods Cell Biol.* 24:97–131.
19. Pryer, N. K., P. Wadsworth, and E. D. Salmon. 1986. Polarized microtubule gliding and particle saltations produced by soluble factors from sea urchin eggs and embryos. *Cell Motil. Cytoskeleton.* 6:537–548.
20. Deleted in proof.
21. Rieder, C. L., E. A. Davison, L. C. W. Jensen, L. Cassimeris, and E. D. Salmon. 1986. Oscillatory movements of monooriented chromosomes and their position relative to the spindle pole result from the ejection properties of the aster and half-spindle. *J. Cell Biol.* 103:581–591.
22. Salmon, E. D., M. McKeel, and T. Hays. 1984. Rapid rate of tubulin dissociation from microtubules in the mitotic spindle in vivo measured by blocking polymerization with colchicine. *J. Cell Biol.* 99:1066–1075.
23. Salmon, E. D., R. J. Leslie, W. M. Saxton, M. L. Karow, and J. R. McIntosh. 1984. Spindle microtubule dynamics in sea urchin embryos: analysis using a fluorescein-labeled tubulin and measurements of fluorescent redistribution after laser photobleaching. *J. Cell Biol.* 99:2165–2174.
24. Salmon, E. D., R. A. Walker, E. T. O'Brien, N. K. Pryer, W. A. Voter, and H. P. Erickson. 1987. Visualization of the polymerization dynamics of individual 25nm-diameter microtubules in real time. Proceedings of the 45th Annual Meeting of the Electron Microscopy Society of America.

G. W. Bailey, editor. San Francisco Press Inc., San Francisco, CA. 636–637.
25. Sammak, P. J., and G. G. Borisy. 1988. Direct observation of microtubule dynamics in living cells. *Nature (Lond.)*. 332:724–726.
26. Sammak, P. J., G. J. Gorbsky, and G. G. Borisy. 1987. Microtubule dynamics in vivo: a test of mechanisms of turnover. *J. Cell Biol.* 104: 395–405.
27. Saxton, W. M., D. L. Stemple, R. J. Leslie, E. D. Salmon, M. Zavortink, and J. R. McIntosh. 1984. Tubulin dynamics in cultured mammalian cells. *J. Cell Biol.* 99:2175–2186.
28. Schliwa, M. 1984. Mechanisms of intracellular organelle transport. *Cell Muscle Motil.* 5:1–82.
29. Schulze, E., and M. Kirschner. 1986. Microtubule dynamics in interphase cells. *J. Cell Biol.* 102:1020–1031.
30. Schulze, E., and M. Kirschner. 1987. Dynamic and stable populations of microtubules in cells. *J. Cell Biol.* 104:277–288.
31. Soltys, B. J., and G. G. Borisy. 1985. Polymerization of tubulin in vivo: direct evidence for assembly onto microtubule ends and from centrosomes. *J. Cell Biol.* 100:1682–1689.
32. Travis, J. L., and S. S. Bowser. 1988. Optical approaches to the study of Foraminiferan motility. *Cell Motil. Cytoskeleton.* 10:126–136.
33. Travis, J. L., J. F. X. Kenealy, and R. D. Allen. 1983. Studies on the motility of the foraminifera. II. The dynamic microtubular cytoskeleton of the reticulopodial network of *Allogromia laticollaris*. *J. Cell Biol.* 97: 1668–1676.
34. Vigers, G. P. A., M. Coue, and J. R. McIntosh. 1988. Fluorescent microtubules break up under illumination. *J. Cell Biol.* 107:1011–1024.
35. Wadsworth, P., and E. D. Salmon. 1986. Analysis of the treadmilling model during metaphase of mitosis using fluorescence redistribution after photobleaching. *J. Cell Biol.* 102:1032–1038.
36. Walker, R. A., E. T. O'Brien, N. K. Pryer, M. F. Soboeiro, W. A. Voter, H. P. Erickson, and E. D.Salmon. 1988. Dynamic instability of individual, MAP-free microtubules analyzed by video light microscopy: rate constants and transition frequencies. *J. Cell Biol.* 107:1437–1448.